Extreme Mechanics Letters 57 (2022) 101921

Contents lists available at ScienceDirect

Extreme Mechanics Letters

journal homepage: www.elsevier.com/locate/eml

Investigation and understanding of the mechanical properties of MXene by high-throughput computations and interpretable machine learning

Shun Tian [a], Ke Zhou [a,*], Chuan-Qi Huang [b], Chen Qian [c], Zhibin Gao [d], Yilun Liu [a,*]

[a] Laboratory for Multiscale Mechanics and Medical Science, SV LAB, School of Aerospace, Xi'an Jiaotong University, Xi'an 710049, China
[b] Hangzhou Institute of Advanced Studies, Zhejiang Normal University, Hangzhou 311231, China
[c] Department of Mechanical Engineering, Zhejiang University, Hangzhou 310058, China
[d] State Key Laboratory for Mechanical Behavior of Materials, Xi'an Jiaotong University, Xi'an 710049, People's Republic of China

ARTICLE INFO

Article history:
Received 5 September 2022
Received in revised form 2 November 2022
Accepted 3 November 2022
Available online 9 November 2022

Keywords:
MXene
2D materials
Tensile stiffness
Strength
Mechanical properties
Interpretable machine learning

ABSTRACT

2D transition metal carbides, nitrides, and carbonitrides (MXenes) have become prominent in energy storage, catalysis, environmental and nanoelectronics applications. In addition to their outstanding merits of electrical conductivity and electrochemically activity, the mechanical properties play crucial roles in all these applications but are usually ignored by researchers. Only quite a few publications have studied their mechanical properties and these studies still only represent a limited range of predictions compared to the large family of MXenes. Utilizing high-throughput computations and data-driven methods, this work studies the tensile stiffness (E^{2D}) and strength (σ_s) of 157 types of MXenes that could be potentially fabricated. We find MXenes with the tensile stiffness ranging from 81.71 to 561.4 N/m, while 42 structures show higher stiffness than the well-known graphene and transition metal dichalcogenide (TMDs) monolayers. The E^{2D} strongly depends on the thickness, bond strength and surface terminations. Surprisingly, we find that the surface terminations can significantly improve the E^{2D}, and the improvement can reach nearly 100%. By using the recently developed interpretable machine learning method, we obtain the analytical formula of E^{2D} with efficient and physically interpretable descriptors that can predict the stiffness accurately. As for the σ_s, it significantly scales with E^{2D} ($\sigma_s \approx E^{2D}/\beta$, $\beta = 10.449$), and can be also improved by surface terminations as well as E^{2D}. In addition, we also find a few of MXene semiconductors, although most of MXenes are metals. Moreover, the mechanical properties of these MXenes are better than the widely used monolayer semiconductor TMDs. These MXenes semiconductors with a moderate band gap may open a new avenue for fabricating next-generation 2D nanoscale electronics, such as all-in-one monolayer devices.

1. Introduction

With the rise of two-dimension (2D) transition metal carbides, nitrides, and carbonitrides (known as MXenes) since 2011, it has grown to prominence in energy storage, catalysis, nanoelectronics, nanofluidics, environmental and biomedical applications because of the attractive physicochemical properties [1–7]. The MXene monolayers are formulated as $M_{n+1}X_nT_x$, which describes alternating $(n+1)$ layers of early transition metals (M=Ti, Zr, Nb, V, and so on) interleaved with n layers of carbon and/or nitrogen (X) with surface functional groups (for example, hydroxyl, oxygen or fluorine) on the exterior transition metal surfaces (Fig. 1a) [2]. Being distinct from other 2D materials, such as the well-known graphene and boron nitride (BN), MXenes have plenty of room to tune the properties through the diversified structures or chemical components of transition metals, carbon/nitrogen, and surface functionalities, which make MXene become the largest family of 2D materials. By now more than 40 types of MXene can be fabricated experimentally and the family is still steadily expanding [8].

Because of the high metallic electrical conductivity (that can reaching to $\approx$ 20,000 S·cm^{-1}) [9], the MXene monolayers can be used as ideal 2D building blocks to create film-like flexible electrodes without a metal current collector in the energy storage devices, which is especially advantageous for nanoelectronic devices when the size is down to micro-/nanometer scale [6]. In these applications, the mechanical properties of MXenes are fundamental, which can control the structural stability of the electrode to withstand expansion and contraction deformation during charge and discharge cycles [1]. Additionally, the MXene

* Corresponding authors.
E-mail addresses: zhouke@xjtu.edu.cn (K. Zhou), yilunliu@mail.xjtu.edu.cn (Y. Liu).

https://doi.org/10.1016/j.eml.2022.101921
2352-4316/

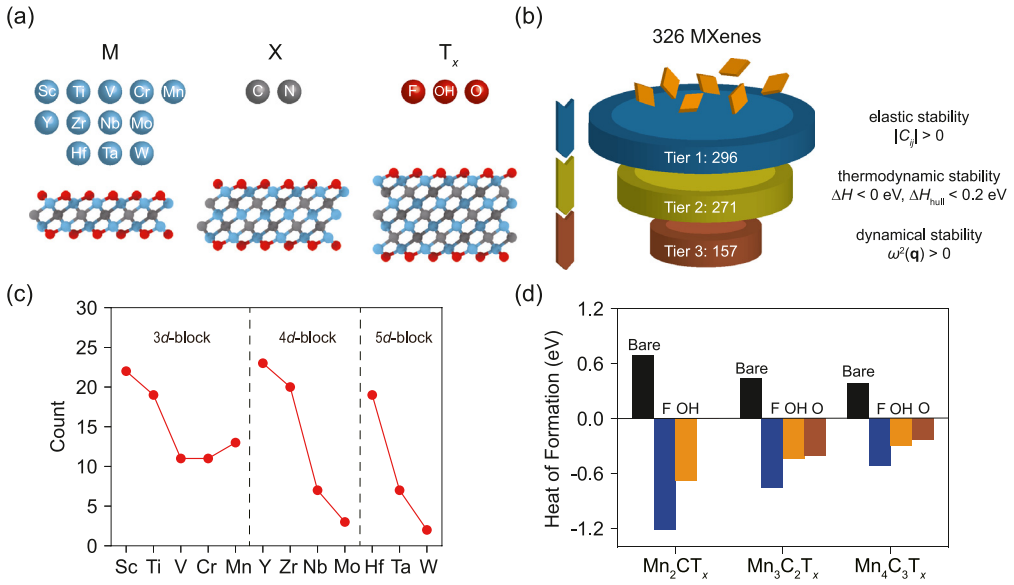

Fig. 1. (a) The structures and compositions of MXenes. A schematic diagram of structures from $n = 1$ to 3 and the elements of M, X and T_x. (b) The screening process. Tier 1: MXenes with negative eigenvalues of elastic tensor were filtered out, which resulted in a reduction from 326 to 296 crystals. Tier 2: MXenes with high thermodynamic stability were reserved, thereby resulting in a reduction from 296 to 271. Tier 3: MXenes with phonon dynamic stability were reserved, finally we obtained 157 stable MXenes that could be potentially synthesized. (c) The distribution of stable MXenes with different M. (d) The heat of formation for $Mn_{n+1}C_nT_x$.

can be used as a reinforcement phase in composite films that the mechanical properties of MXene to withstand the required mechanical loading while maintaining the functions for these applications is important [10,11]. The Young's modulus (E) or tensile stiffness (E^{2D}, $E^{2D} = E \times h$, h is the thickness of 2D materials) is the most important mechanical parameter for engineering materials, which measures the ability to withstand the changes in length when under tension or compression. The value of E or E^{2D} is directly relevant to bending stiffness (D, $D \sim Eh^3$ according to the theory of plates and shells, or $D \sim Eh^2$ according to the recently developed theory) [12] and idea strength (σ_s, $\sigma_s \approx E/10$) [13]. Despite extensive works about MXenes since their discovery, only a few publications have studied their mechanical properties [14–17], especially for experimental work (only 2 works by now [16,17]). Density functional theory (DFT) calculations have been conducted to calculate the mechanical properties for some MXenes [18–20], but these studies still only represent a limited range of predictions as compared to the large number of the MXene structures. This highlights the necessity for high-throughput calculations to explore the essential principles of MXenes' mechanical properties.

With the accumulated database generated by extensive DFT calculations, the data mining and machine learning methods become cheap and efficient tools for material discovery and investigation, accelerating the searching and understanding of materials with remarkable properties [21–24]. Recently developed 2D materials databases, such as Computational 2D Materials Database (C2DB) [25], the 2D Materials Encyclopedia (2DMatPedia) [26] and the Joint Automated Repository For Various Integrated Simulations (JARVIS) [27], contains 4047, 6351 and 1079 2D materials, respectively. These large databases make the investigation of the mechanical properties of MXenes possible. The C2DB database includes 326 MXenes with various structural, thermodynamic, elastic, electronic, magnetic, and optical properties [25]. This potentially allows us to do high-throughput calculations to study the mechanical behavior of MXenes.

To explore the essential principles of mechanical properties of MXenes, we study the 157 types of MXenes (selected from 326 types of MXenes in the C2DB database) that could be potentially fabricated by experiments using high-throughput computations and data-driven methods. We derive the in-plane tensile stiffness from the stiffness tensors provided in C2DB. We find that MXenes possess E^{2D} ranging from 81.71 to 561.4 N/m and 42 among these structures show higher values than the well-known graphene, h-BN and transition metal dichalcogenide (TMDs) monolayers. The E^{2D} strongly depends on the thickness (h), stiffness of M–X bonds and surface terminations that cannot be understood by the classical continuum mechanics that predicts $E^{2D} \sim h$. The presence of surface terminations can increases the loading area or thickness while weakening the inner M–X bonding strength. Surprisingly, we find that the surface terminations can significantly improve the E^{2D} of bare MXenes and the improvement can reach nearly 100%. Using the recently developed interpretable machine learning method, known as the sure independence screening and sparsifying operator (SISSO) method, we obtain the analytical formula of E^{2D} with efficient and physically interpretable descriptors, which can predict the E^{2D} accurately. As for the σ_s, it significantly scales with E^{2D} ($\sigma_s \approx E^{2D}/\beta$, $\beta = 10.449$), and can also be improved by surface terminations as E^{2D}. Here, we also find a few of MXenes are semiconductors although most of MXenes are metallic. Moreover, the mechanical properties of these MXenes are better than the widely used monolayer semiconductor TMDs. These MXenes semiconductors with a moderate band gap may open a new avenue for fabricating next-generation 2D nanoscale electronics, such as all-in-one monolayer devices. Along with the mechanical-strengthening effects of surface terminations, terminations engineering can be a promising tool in the field of MXenes.

2. Results

Criteria of Stability. To date, C2DB includes structural and stability information of 326 MXenes with $n = 1$, 2 and 3. The structures in the C2DB are generated by a combinatorial method [25], which inevitably produces many unstable materials that cannot be successfully fabricated. Here, we adopted a set of stability criteria to quantify the stability of MXene as our previous work [24] (see Fig. 1). (1) According to the Born criteria of elastic stability [28], the definite of the stiffness matrix of materials (C_{ij}) should be

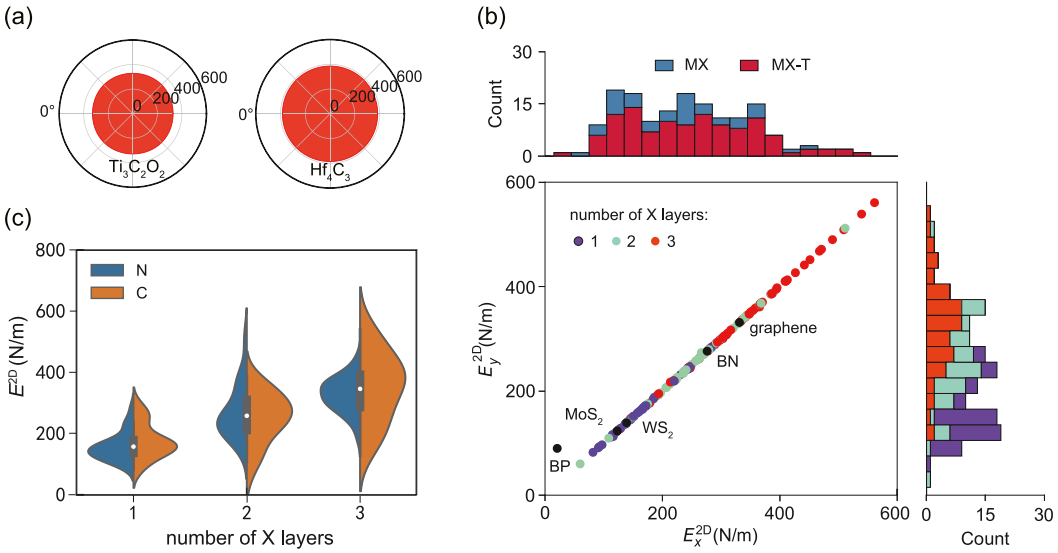

Fig. 2. (a) The orientation-dependent stiffness ($E^{2D}(\theta)$) of $Ti_3C_2O_2$ and Hf_4C_3. (b) The distribution of the in-plane stiffness for 157 stable MXenes along the x (E_x^{2D}) and y (E_y^{2D}) direction. The colors of points indicate the number of carbon/nitrogen (X) layers. The E^{2D} of other typical monolayer 2D materials (here are graphene, BN, WS_2, MoS_2 and black phosphorus (BP)) are also shown in the figure as black dots. (c) The violin plot of statistical results of E^{2D} that showing the effects of the type of X and the number of X atomic layers. The blue and orange represent nitride and carbide MXene, respectively. The white dots in the middle represent the median value and the thick black bar in the center represents the interquartile range. (For interpretation of the references to color in this figure legend, the reader is referred to the web version of this article.)

positive, that is $|C_{ij}| > 0$ or all the eigenvalues of C_{ij} is positive (Tier 1). (2) The thermodynamic stability can be divided into three levels (high, medium and low) according to the value of heat of formation ΔH and energy above convex hull ΔH_{hull} [25]. The *high* thermodynamic stability requires $\Delta H < 0$ eV/atom and $\Delta H_{\text{hull}} < 0.2$ eV/atom, which can be considered as stable and potentially synthesizable materials. *Medium* thermodynamic stability means $\Delta H < 0$ eV/atom but $\Delta H_{\text{hull}} > 0.2$ eV/atom. Material with $\Delta H > 0$ has *low* thermodynamic stability. In this work, we only consider the MXene with high thermodynamic stability (Tier 2). (3) For a material to be dynamically stable, it is necessary and sufficient that all its phonon modes have positive frequencies for all wave vectors $\mathbf{q}$ ($\omega^2(\mathbf{q}) > 0$, Tier 3). With this screening process, 157 types of MXenes are obtained that could be potentially synthesized. According to the reported results, we find that some MXenes have been successfully synthesized [8,14], which means the stability criteria used in this work are reliable. One point should be noted that some MXenes not included in C2DB can be also synthesizable, such as the MXene with Janus surface terminations and the high entropy MXene found recently [29–31].

The Stable MXene. The information of each stable MXene identified by our screening process is included in **Supplemental Files**. We find the number of each kind of M-containing MXenes tends to decrease as the increase of the group number of M in the same period as shown in Fig. 1c. As a result, Sc, Y and Hf have the largest number of stable MXenes in the 3*d*, 4*d* and 5*d* transition metal blocks, respectively. This indicates that MXenes composed of light transition metals are more likely to be stable. However, Cr and Mn do not follow this trend that the number of stable MXene is not less than V. In order to clarify this anomaly, we counted the number MXenes that were filtered out due to dynamical and thermodynamic stability. We find that the increase of group number of M in the same period can result in a significant increase of the number of MXenes with phonon instability (Fig. S1a), which could explain the downward trend in Fig. 1c. Nevertheless, for Mn and Cr, the amount of both phonon and stiffness dynamically unstable MXenes is abnormally small. Moreover, we found that functional groups can improve the stability of MXenes. Taking Mn-carbides as an example (shown in Fig. 1d), bare Mn-carbides MXenes are thermodynamically unstable owing to their positive formation energy. However, their functional states are thermodynamically stable due to the negative formation energy. In addition, there are more carbide MXenes than nitride MXenes among all the stable MXenes generally, which means X also affects the stability (Fig. S1b).

The Stiffness of MXene. After screening out MXenes that satisfy the stability criteria, we further study the in-plane tensile stiffness (E^{2D}), which is one of the most important mechanical properties of materials. The orientation-dependent $E^{2D}(\theta)$ can be derived from the elastic tensors (C_{ij}, see details in **Methods**) [32]. Because the structure of MXenes is hexagonal symmetry, the MXene is elastic isotropy (taking $Ti_3C_2O_2$ and Hf_4C_3 as examples, as shown in Fig. 2a), which means $E_x^{2D} = E_y^{2D} = E^{2D}$ (Fig. 2b). We can find a few points in Fig. 2b depart slightly from the diagonal, which attributes to the calculation error of elasticity tensors. Here one point should be noted that elasticity isotropy cannot guarantee strength isotropy of MXene that we will discuss in the **Discussion** section. The E^{2D} of the stable MXenes ranges from 81.71 to 561.409 N/m, 42 of these stable MXenes possess a higher stiffness than the well-known graphene (331.2 N/m). The large range of stiffness is due to MXene's diverse structures and chemical compositions. The chemical formula of the most rigid MXenes are $M_4C_3O_2$ such as $Ta_4C_3O_2$, $Nb_4C_3O_2$ and $V_4C_3O_2$, while the least rigid MXenes have a chemical formula of M_2X such as Y_2N, Sc_2C and Y_2C. We can tell directly that the MXenes with $n = 3$ indicated by red dots are mainly distributed on the top, followed by the MXenes with $n = 2$ indicated by aquamarine dots in the middle and the MXenes with $n = 1$ labeled by blue dots at the bottom. It can also be found from the distribution of E^{2D} splitting on the layers as shown on the right. It directly indicates the thickness effect on the stiffness of MXenes. The violin plot of Fig. 2c also confirms this finding statistically that the E^{2D} increases with the number of X layers for both carbides and nitrides MXene. In addition, we also find that the average E^{2D} of carbides MXene is a little larger than the nitrides counterparts (Fig. 2c), which means the minor effect of X atoms on the E^{2D}.

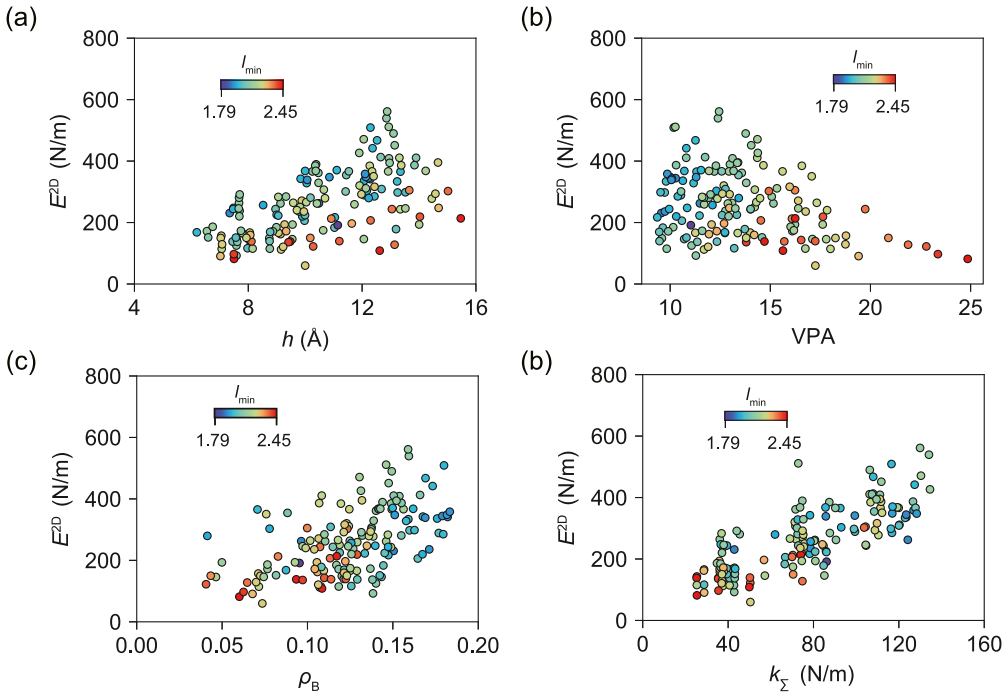

Fig. 3. The relation between E^{2D} and (a) thickness (h), (b) volume per atom (VPA), (c) bond density (ρ_B) and (d) sum of all the bond stiffness (k_Σ). The colors of points indicate the minimum bond length (l_{min}).

According to the classical continuum mechanics, the in-plane stiffness is positively correlated to the thickness, that is $E^{2D} \sim h$. Here, we define the thickness (h) of MXenes as a geometric method, $h = d_{T-B} + r_T + r_B$, where d_{T-B} is the sum of the vertical distance between the topmost and bottommost atoms, r_T and r_B is the van der Waals radius of the topmost and bottommost atoms, respectively. Although there exist other definitions [33], the geometric definition is valid for 2D materials (see details in Fig. S2 and Table S1). The relation between E^{2D} and h in Fig. 3a shows that E^{2D} is positively correlated with h generally but the data is scattering, especially at large h. This means there are factors beyond the h determining the values of E^{2D}. Volume per atom (VPA) defines as the ratio of volume (defined as the cross-section area times h) to the number of atoms, which can be the measurement of cohesive strength of materials because it is correlated with the bond strength and bond length [34,35]. The small value of VPA means the atoms in materials are tight and the large means loose. Fig. 3b shows that MXenes with high VPA tend to possess low E^{2D}, which is consistent with the previous study on Young's modulus of bulk materials [21]. We also plot the relation between E^{2D} and bond density (ρ_B, defined as the number of bonds in the unit volume) that MXenes with high E^{2D} tend to possess high ρ_B but also shows large scatter, as illustrated in Fig. 3c. Because the specificity of M–X bonds is ignored in the definitions of h, PVA and ρ_B, all the scaling with E^{2D} is ambiguous. In this work, we find the total bond strength (k_Σ) of all the M–X and M–T_x bonds in the primitive cell can be a better descriptor for E^{2D} (Fig. 3d) that $E^{2D} \sim k_\Sigma$ with much little scatter compared to h, VPA and ρ_B. This can be understood that the specificity of bonds can be explicitly included in k_Σ while it is hidden in the definitions of other descriptors. Here we color the points Figs. 3a–d coding by the minimum bond length (l_{min}) that MXenes with a small l_{min} tend to have a large E^{2D}, which also indicates that the bond stiffness has a great influence on E^{2D} (short bond length means large bond stiffness generally). In this work, the bond strength is characterized through the bond stiffness, which can be derived from the bond energy and bond length empirically as in previous work [14]. Tables S2 and S3 summarize the bond energies, bond length and bond stiffness of M–X bonds and M–T_x. The data of the bond energy comes from reported work [36].

Improvement of Stiffness by Surface Terminations. The surfaces of MXene are always covered by the surface terminations as the result of chemical etching. After the screening process (Fig. 1), 38 kinds of stable bare MXenes have corresponding stable functional states. Fig. 4a shows the E^{2D} of MXenes with and without surface terminations. Surprisingly, we find the surface terminations can significantly improve the E^{2D} of bare MXenes and the improvement can reach nearly 100% (such as $Mn_4N_3O_2$). This result is reverse to graphene that functional groups on the surface can significantly worsen the mechanical properties. Among the three types of functional groups, we find the improvement of O groups is better than OH and F groups statistically (Figs. 4a and b). While the improvement of OH and F groups are quite similar (see Fig. S3). Intuitively, the improvement on the E^{2D} could be from the increase of the thickness because of the introduction of surface terminations. Here we plot the relation between $E^{2D}_{MX-T}/E^{2D}_{MX}$ and $h^{2D}_{MX-T}/h^{2D}_{MX}$, which means the improvement of E^{2D} and thickness, where E^{2D}_{MX-T} (h^{2D}_{MX-T}) and E^{2D}_{MX} (h^{2D}_{MX}) is the stiffness (thickness) of MXenes with and without surface terminations, respectively. It should be $E^{2D}_{MX-T}/E^{2D}_{MX} \sim h^{2D}_{MX-T}/h^{2D}_{MX}$ if $E^{2D} \sim h$. While we find only a small part of points are near the diagonal in Fig. 4b and most points are located at higher positions. For example, the E^{2D} of Zr_2NO_2 (220.3 N/m) is 1.7 times of the bare Zr_2N (129.2 N/m), but the thickness of Zr_2NO_2 (7.69 Å) is only 1.09 times of Zr_2N (7.08 Å). The underestimation of E^{2D} by h can be understood that the scaling between bonds in bare MXenes (that is M–X bonds) and surface bonds to h is different (see Fig. 4b–c). Here we also plot the relation between $E^{2D}_{MX-T}/E^{2D}_{MX}$ and $k^{MX-T}_\Sigma/k^{MX}_\Sigma$ that latter means the improvement of total bond stiffness (Fig. 4c), where k^{MX-T}_Σ and k^{MX}_Σ is the total bond stiffness of MXenes with and without surface terminations, respectively. It should be $E^{2D}_{MX-T}/E^{2D}_{MX} \sim k^{MX-T}_\Sigma/k^{MX}_\Sigma$ according to the conclusion in the last section. While we find most of the points locates under the diagonal as shown in Fig. 4c. For example, the E^{2D} of $Ta_3C_2O_2$ (385.02 N/m) is 1.35 times of Ta_3C_2 (284.54 N/m), but the k_Σ

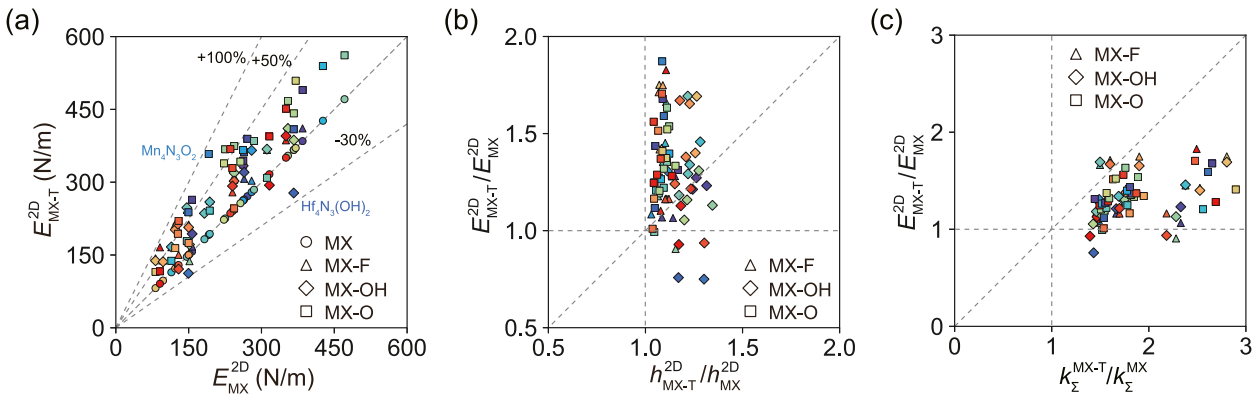

Fig. 4. (a) The results of E^{2D} with and without surface terminations. The change of E^{2D} at different levels (+100%, +50%, and −30%) is shown as dash lines. (b) The relation between the modification of h ($h^{2D}_{MX-T}/h^{2D}_{MX}$) and the improvement of E^{2D} ($E^{2D}_{MX-T}/E^{2D}_{MX}$). (c) The relation between the modification of k_Σ ($k_\Sigma^{MX-T}/k_\Sigma^{MX}$) and the improvement of E^{2D}. Here, different colors mean different types of MX.

of $Ta_3C_2O_2$ (142.5 eV/Å^2) is 1.81 times of Ta_3C_2 (78.48 eV/Å^2). The overestimation of E^{2D} by k_Σ means there is a coupling effect between inner bonds and surface bonds. Moreover, we can infer this coupling effect plays a negative contribution to stiffness.

The results above mean the mechanism of improvement on the E^{2D} can be beyond the effects of h and k_Σ. Some modifications could exist in the structure and interaction inside of MXene. In this work, we mainly focus on the MXene of $M_3C_2T_x$ ($n = 2$) as representatives to discuss the effect of surface terminations on the modification. Here we define the *inner* M–C bonds as the M_1-C bond in the center of MXene and the *outer* M–C bonds as the M_2-C bond near the surface. The results in Fig. S4a–b show that the M_2-C bonds become longer while the M_1-C bonds become shorter compared to their bare counterparts, which means the strengthening of inner bonds and the weakening of outer bonds according to the empirical expression of bond stiffness (see details in Table S2). Here, we also calculate the bond strength by the crystal orbital Hamilton population (COHP) analysis [37]. The results as shown in Fig. S5 show that the bond strength of *outer* bonds is weakened while *inner* bonds are strengthened in general. Here, we attribute the change of bond length to charge transfer modulated by surface terminations (Fig. S4c–f). The negatively charged functional groups mean they can gain electrons from the inner atoms of MXenes. By using Bader charge analysis [38], we find that the atomic charges on M_1 atoms of functionalized MXenes tend to increase slightly, while the atomic charges on M_2 atoms increase significantly. As for C atoms of functionalized MXenes, the atomic charges tend to increase. Such charge redistribution could weaken the outer M–C bonds and strengthens the inner M–C bonds, which makes the outer M–C bonds become longer while inner M–C bonds become shorter compared to their bare counterparts. These conclusions above are also valid for MXenes with $n = 1$ and 3 (see details in Figs. S6 and 7).

3. Discussion

The Formula of E^{2D} from Interpretable Machine Learning. According to the understanding above, the E^{2D} correlates with the thickness or number of X layers (n, directly representing the number of internal bonds), the strength of bonds and surface terminations. Here, we also perform correlation analyses for these 3 factors along with others, such as average bond length, average atomic radius, volume per atom and so on. The results of Fig. S8 confirm our conclusions above are reliable. In order to get the formula of E^{2D}, we use the recently developed SISSO method, which is a compressed sensing-based methodology generating predictive models and expressed as interpretable formulas [39]. SISSO combines the sure-independence screening (SIS) and sparsifying operators (SO) algorithm to obtain the best descriptors for E^{2D} and the results are same as our conclusions. Here, we get the formula of E^{2D} as following,

$$E^{2D} = E_{MX} + E_{coupling} + E_{Tx} \quad (1)$$

where $E_{MX} = 5.92\times n\times k_{M-X}$, $E_{coupling} = -0.036\times n\times k_{M-X}\times k_{M-T}$, and $E_{Tx} = 12.27 \times k_{M-T} - 192.23$. n is the stoichiometry of the MXene $M_{n+1}X_nT_x$, k_{M-X} is the bond stiffness of M–X bond, and k_{M-T} is the bond stiffness of M–T_x bond. Here all the parameters are dimensionless numbers and the unit of E^{2D} is N/m. This formula has clear physical insights and is well explainable. The first term E_{MX} represents the effect of thickness and bond stiffness of internal M–X bonds with the positive contribution. The second term $E_{coupling}$ with a negative coefficient means the weakening effect of surface terminations on internal M–X bonds. The third term E_{Tx} means the contribution of M–T_x bonds with the positive contribution. For bare MXenes, the E^{2D} is directly equal to E_{MX}. All of these are well consistent with our conclusions above. The E^{2D} predicted from Eq. (1) is plotted against the DFT results (Fig. 5a). The points located near the diagonal in general with the root mean squared error and the coefficient of determination (R^2) of 49.64 and 0.776, which indicates the successful prediction of Eq. (1). By using Eq. (1), we can get the contributions of the three terms that the first and third terms are dominant (Fig. S9). One point should be noted that the stiffness of internal M–X bonds may be different. As mentioned in the previous section, the surface terminations can strengthen the internal M–X bonds while weakening the outer M–X bonds for MXenes with $n = 2$ and 3. Here, we use the same parameters (Table S2) for both inner and outer M–X bonds for convenience, but this would bring errors to the prediction of E^{2D}.

To further explore the significance of the obtained formula, the E^{2D} is plotted as a function of $n \times k_{M-X}$ and k_{M-T} using Eq. (1) (Fig. 5b). The values of k_{M-X} range from 12.09 to 21.48 eV/(A^2) according to the handbook of chemical energies [36], while the M–T bonds range from 0 to 32.01 eV/(A^2) (the bare MXenes with a k_{M-T} of zero). Fig. 5b shows that the lower and upper bounds of E^{2D} are ≈ 80 and ≈ 560 N/m in the case of $n = 1-3$, which is in perfect agreement with the DFT results (81.72 to 561.41 N/m). Furthermore, we can predict the E^{2D} and Young's modulus (E) of MXenes in cases of $n = 4-10$ that the data is absent in the C2DB data and are rarely studied by now. One point should be noted that we can only fabricate MXenes with $n = 1-3$ now. The results shown in Fig. 5c exhibit a strong thickness effect on E^{2D} and the highest value can reach 1296.35 N/m when $n = 10$

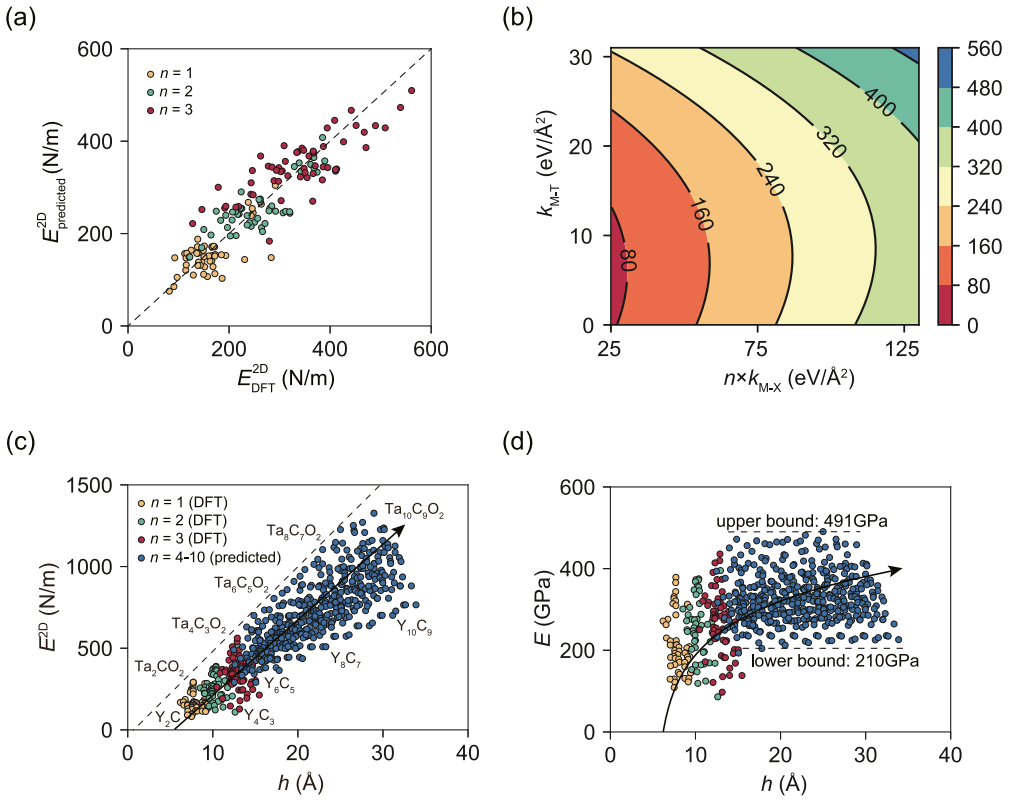

Fig. 5. (a) The predicted E^{2D} against DFT results. Different colors mean the stoichiometry of n. (b) The predicted E^{2D} as a function of $n \times k_{M-X}$ and k_{M-T}. (c) The predicted E^{2D} as a function of h when $n = 4-10$ along with the DFT results of $n = 1-3$. (d) The predicted Young's modulus (E). The black lines with the arrow in (c) and (d) are the guidelines.

($Ta_{10}C_9O_2$). More importantly, our DFT calculation and predicted results show that the stiffest MXenes have a common chemical formula of $Ta_{n+1}C_nO_2$ at different n, which is due to the strong bonds between Ta and C or O elements. We also find the intercept of $E^{2D}(h)$ relation is smaller than zero, which can be understood that the h (that includes the van der Waals radius of the topmost and bottommost atoms) is a finite value. In addition, we find Young's modulus E increases with the thickness h and converges between 210 to 491 GPa when $n > 4$ (Fig. 5d). This is due to the factor $\alpha > 1$ for the scaling $E^{2D} \sim h^{\alpha}$ for n=1 to 3, which can be proved from Fig. 4b that most points are distributed above the diagonal. We also found that $V_{n+1}N_nT_x$ and $Ta_{n+1}N_nT_x$ MXenes such as $V_{10}N_9$ and $Ta_{10}N_9O_2$ have the maximal E (for $n = 1, 2, 3$, and $n > 3$). The gravimetric moduli of MXene range from 23.74 to 91.35 GPa$\times$g^{-1}cm^3, which is much smaller than the theoretical bounds [40].

The Strength of MXenes. The theoretical strength (σ_s) is the upper strength limit that materials can withstand [43] and is another important parameter except for stiffness. Not like E^{2D}, which is isotropic, the strength of σ_s of MXenes is orientation-dependence because the symmetry of the structure is broken when deformation. For example, $Ti_3C_2O_2$ possesses a higher strength in the zigzag direction that could be due to different bond densities in two directions. In this work, we only calculate the σ_s in two high-symmetry directions, that is along the x (armchair) and y (zigzag) directions as shown in the inset in Fig. 6a. Because the σ_s calculated by stress–strain curves cost a lot of computation resources, we only calculate the MXenes with $n = 2$ (that is widely used in experiments) for further discussion. Fig. 6a shows the calculated stress–strain curves of $Ti_3C_2T_x$ under uniaxial tensile. It can be seen that all functionalized $Ti_3C_2T_2$ possess much higher σ_s than that of bare counterparts in both armchair and zigzag directions (see details in Table S4). Among three types of surface terminations, the MXenes with the oxygen group tends to show the most enhancement of MXene's strength (i.e., 46.01 N/m for $Hf_3C_2O_2$ versus 38.61 N/m for $Hf_3C_2OH_2$ and 36.42 N/m for $Hf_3C_2F_2$ in the zigzag direction). These conclusions are valid for other MXenes (see details in Figure S10 and Table S5).

As shown in Figure S11, we find that the σ_s exhibit periodicity similar to stiffness and the MXenes with Ti, Nb and Ta in the 3*d*, 4*d* and 5*d*-block transition metals tend to have the highest σ_s. It is reminiscent of the estimation of σ_s from Griffith theory ($\sigma_s \approx E/9$) or Frenkel and Orowan–Polanyi's model ($\sigma_s \approx E/10$) that connects the relation between stiffness and strength [41,42]. Our results illustrated in Fig. 6c indicates that the σ_s have an upper bound of $E^{2D}/6$ and a lower bound of $E^{2D}/18$. The σ_s of some MXenes such as $Zr_3C_2O_2$ and $Hf_3C_2O_2$ exceed the $E^{2D}/9$ predicted by the Griffith theory in the zigzag directions. We also fit the relation between σ_s and E^{2D} by $\sigma_s = E^{2D}/\beta$ that the resulting $\beta = 10.449$ (with $R^2 = 0.584$). In addition, we summarize the σ_s and fracture strain (ε_s) in Fig. 6d. We find most of MXenes have higher σ_s than the transition metal dichalcogenides (TMDs) monolayers. Moreover, there are many types of MXenes process with comparable or better mechanical properties than well-known graphene and *h*-BN. Thus, MXenes can be promising alternatives for the devices requiring strong materials, which have been already used in recent works [6,10,11,44,45]. Moreover, with the merit of electrical conductivity (for most of MXenes), they can be ideal interconnects for nanoscale electronics that link electronic nodes in an integrated circuit with excellent mechanical properties and atomic thickness [44].

The Avenue towards *All-in-One* Monolayer Nanoscale Electronics. Because of highly metallic conductivity, MXenes have demonstrated state-of-the-art performance in energy storage, electromagnetic shielding and chemical sensing. Although most

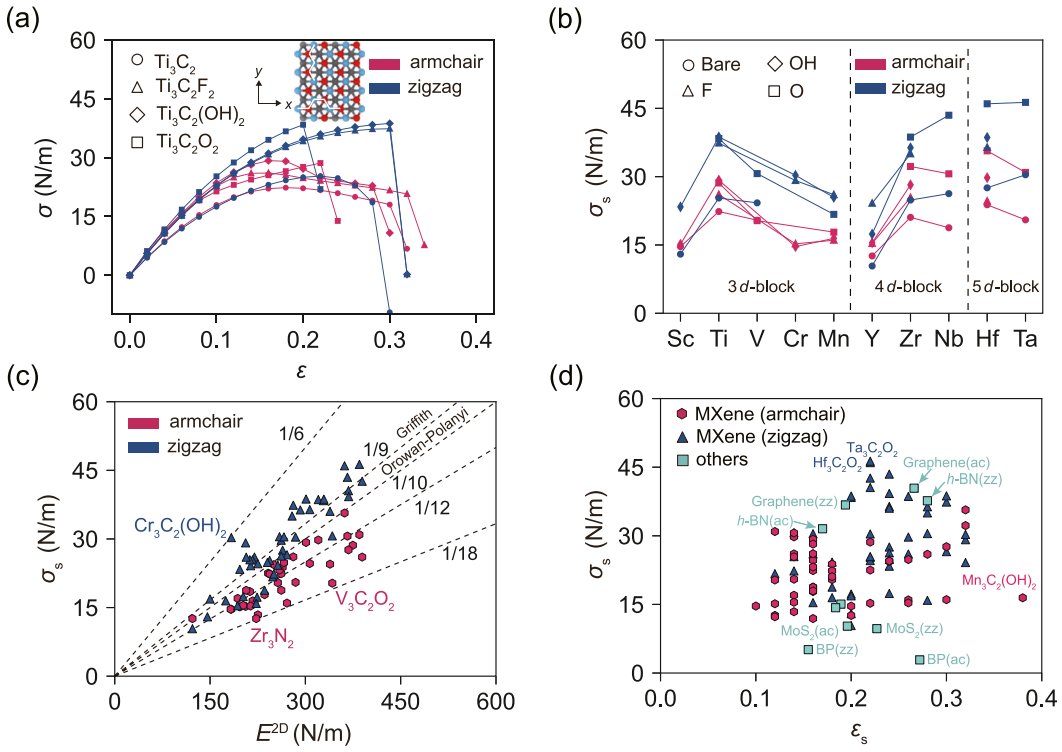

Fig. 6. (a) The uniaxial tension strain–stress curves of Ti_3C_2,$Ti_3C_2F_2$,$Ti_3C_2(OH)_2$ and $Ti_3C_2O_2$ in both armchair and zigzag directions. (b) Calculated tensile strength of all stable $M_3C_2T_x$ MXenes in both armchair and zigzag directions. (c) The results of σ_s and E^{2D} of stable $M_3X_2T_x$ MXenes. The ratio of σ_s/E^{2D} at different levels (1/6, 1/9, 1/10, 1/12, 1/18) is shown as dash lines. 1/9 and 1/10 is the prediction from Griffith theory and Frenkel and Orowan–Polanyi's model, respectively [41,42]. (d) The tensile strength (σ_s) versus fracture strain (ε_s) of $M_3X_2T_x$ MXenes and other 2D materials such as graphene, MoS_2, black phosphorus and *h*-BN. Here ac and zz mean armchair and zigzag direction, respectively.

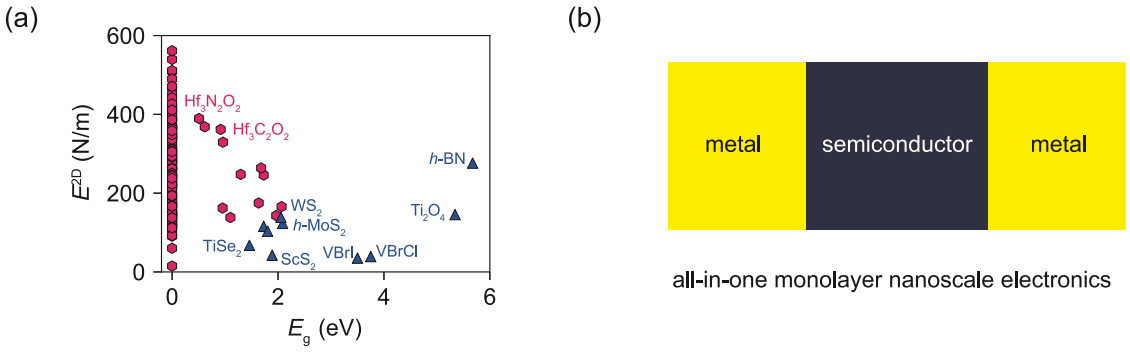

Fig. 7. (a) The distribution of band gap E_g (calculated under the level of HSE06 [25]) and stiffness. (b) The concept of all-in-one monolayer electronics that semiconductors and electrodes (or interconnects) are all made by MXene with different surface terminations.

of MXenes are metallic [25], there are also a few MXenes are semiconductors (Fig. 7a). Moreover, the mechanical properties of some MXenes are better than the widely used monolayer semiconductor TMDs. These MXenes semiconductors with a moderate band gap (E_g) may open a new avenue for fabricating next-generation 2D nanoscale electronics. For example, Hf_2CO_2 has higher E^{2D} along with a higher thermal conductivity than that of phosphorene or MoS_2, and high carrier mobility comparable to that of phosphorene [46]. Here, we find some MXenes with one type of surface termination is metallic but can be a semiconductor with other terminations. For example, Ti_2CO_2 and Hf_2CO_2 are semiconductors with $E_g = 1.295$ and 1.729 eV, respectively. While Ti_2CF_2, $Ti_2C(OH)_2$, Hf_2CF_2 and $Hf_2C(OH)_2$ are metallic. Very Recently, Chi Zhang and co-workers developed an electrochemical treatment method that can control surface terminations of $Ti_3C_2T_x$ switched between an OH-rich form ($Ti_3C_2(OH)_2$) and an O-rich form ($Ti_3C_2O_2$) [47]. This inspires us that we can achieve both metal and semiconductor in one monolayer (Fig. 7b). In this case, we can get *all-in-one* monolayer electronics in which semiconductors and electrodes (or interconnects) are all made by MXene but with different surface terminations. Under this new electronics architecture, the thickness is reduced a lot without metal electrodes or the surface scattering (that can lead to high contact resistance and lowered carrier mobility [48]) between electrodes and semiconductors is eliminated, which is promising in the next-generation computation devices [49].

4. Conclusions

Despite the extensive works about MXenes since their discovery, only a few works have studied their mechanical properties. Moreover, these studies still only represent a limited range compared to the large size of the MXene family. In this work, by using high-throughput computations and data-driven methods,

we study the mechanical properties of MXenes by exploring more than 157 types of MXenes that could be potentially fabricated by experiments. We find MXenes possess excellent tensile stiffness that ranges from 81.71 to 561.4 N/m that 42 of these show higher stiffness than the well-known graphene and TMDs monolayers. The E^{2D} strongly depends on the thickness, stiffness of M–X bonds and surface terminations that cannot be understood by the classical continuum mechanics (that $E^{2D} \sim h$). Surprisingly, we find the surface terminations can significantly improve the E^{2D} of bare MXenes and the improvement can reach nearly 100%. Using the recently developed interpretable machine learning method, we obtain the analytical formula of E^{2D} with efficient and physically interpretable descriptors, which can predict the E^{2D} accurately. As for the σ_s, it strongly scales with E^{2D} ($\sigma_s \approx E^{2D}/\beta$, $\beta = 10.449$) and σ_s can also be improved by surface terminations as E^{2D}. Here, we also find a few of MXenes are semiconductors although most of MXenes are metallic. Moreover, the mechanical properties of these MXenes are better than the widely used monolayer semiconductor TMDs. These MXenes semiconductors with a moderate band gap may open a new avenue for fabricating next-generation 2D nanoscale electronics, such as all-in-one monolayer devices.

Methods

Computation of the in-plane tensile stiffness from elastic tensors. The elastic tensor is a 4-rank tensor, which describes the relationship between strain and stress by the generalized Hooke's law $\sigma_{ij} = C_{ijkl}\epsilon_{kl}$. The number of independent components of C_{ijkl} is 21, which reduces to 6 in 2D [50]. Disregarding shear deformations [18,50], we have

$$\begin{bmatrix} \sigma_{xx} \\ \sigma_{yy} \end{bmatrix} = \begin{bmatrix} C_{11} & C_{12} \\ C_{12} & C_{22} \end{bmatrix} \begin{bmatrix} \epsilon_{xx} \\ \epsilon_{yy} \end{bmatrix}$$

The in-plane stiffness and shear moduli (G), Poisson's ratio (μ) could be derived from elastic constants as:

$$E_x^{2D} = \frac{C_{11}C_{22} - C_{12}C_{21}}{C_{22}}, \quad E_y^{2D} = \frac{C_{11}C_{22} - C_{12}C_{21}}{C_{11}}$$

$$G_{xy}^{2D} = C_{66}, \quad \nu_{xy}^{2D} = \frac{C_{21}}{C_{22}}, \quad \nu_{yx}^{2D} = \frac{C_{12}}{C_{22}}$$

The 2D in-plane stiffness (E^{2D}) and Young's modulus (E) can be transformed as follows, $E = E^{2D}/h$, where h is the thickness of MXenes. There are various definitions of h (see details in **Supplemental Notes**). The geometric thickness can be obtained without extra DFT calculation and thus is used in this work. It is important to note that the h will strongly influence the values of E, while E^{2D} does not rely on the choice of the thickness with various definitions. Therefore, we mainly focused on the discussion of E^{2D} in our work to investigate the effects of compositions and structures on the mechanical properties of MXenes.

DFT calculations. The mechanical properties of MXene are calculated using DFT as implemented by the Vienna *ab initio* simulation package (VASP) [51,52] with spin polarization based on the projector augmented wave method (PAW) [53] and the Perdew–Burke–Ernzerhof (PBE) exchange–correlation functional [54]. Lattice parameters and atomic coordinates are optimized with the energy convergence of 10^{-6} eV/cell, and the criterion for force convergence during the relaxation is 10^{-3} eV/Å. The mesh grid of k-points was adopted as $13 \times 13 \times 1$ for the primitive cell. The cut-off energy for the plane wave is 600 eV. The height of the unit cell in the z direction is approximately 22 Å that ensures the vacuum layer is thick enough. During the calculations of stress–strain relations, the lattice vectors and internal atomic positions are fully relaxed at each pre-set strain to ensure that the MXene is under uniaxial tension. The tensile strain is defined as engineering strain, $\varepsilon = a/a_0$, where a_0 and a are the equilibrium and strained lattice constant, respectively. During the relaxation, the length of the cell along the z direction is intact. The strain step is 2%. The simulated cell was taken from the relaxed structures of the previous step that ensuring the strain path is continuous. According to the generalized Hook's law, the in-plane elastic constants are calculated by applying small strains of ±1% with the increment of 0.5% to the equilibrium configuration, and the elastic constants C_{ij} are derived from the second-order derivative of the total energies versus applied strain using the VASPKIT [55]. The Crystal orbital Hamilton population (COHP) analysis was used to calculate the bond strength using LOBSTER [37,56]. Here, we also perform independent calculations of C_{ij} for some 2D crystals and MXenes (see details Table S7). The resulting E^{2D} is consistent with that calculated from C_{ij} supplied by C2DB, which confirms the data in C2DB is reliable.

SISSO method. We adopted n, k_{M-T} and k_{M-X} as input features (these data could be obtained in **SI**) and E^{2D} as output. The operators set is defined as,

$$\Theta \equiv (+, -, \times, \div, \sqrt{}, ^{-1}, ^{2})[n, k_{M-X}, k_{M-T}]$$

The intrinsically linear relationship observables in the compressed-sensing formalism is made non-linear by equipping the features space non-linear operators Θ. At each iteration, Θ operates on all available combinations, and the features space grows recursively to form a huge feature space. The dimension of the descriptor is set to 3, and the top 1500 potential descriptors most applicable to describe E^{2D} were identified using one iteration of SISSO with a subspace size of 1500.

The structures of MXenes. There are two types of structures of MXene in C2DB (Fig. S12). The one is T phase that could be directly fabricated by selective etching of A-group element on 3D bulk MAX phase. The another is H phase that the structure is symmetry along the center plane [57]. In the C2BD database, the structure for $n = 1$ and 3 is T phase while is H phase for $n = 2$. We believe the mechanical properties are same for both phases because the structures are so similar. Here, we also calculate E^{2D} for the T-phase MXenes with $n = 2$ that the values are the same as the H phase in general (Fig. S13 and Table S6 and S8). Thus, we still use the results of H phase for $n = 2$ in this work.

CRediT authorship contribution statement

Shun Tian: Analyzed data, Writing – original draft. **Ke Zhou:** Conceived and directed the research, Analyzed data, Writing – original draft. **Chuan-Qi Huang:** Analyzed data, Writing – original draft. **Chen Qian:** Analyzed data, Writing – original draft. **Zhibin Gao:** Analyzed data, Writing – original draft. **Yilun Liu:** Conceived and directed the research, Analyzed data, Writing – original draft.

Declaration of competing interest

The authors declare the following financial interests/personal relationships which may be considered as potential competing interests: Yilun Liu reports was provided by Xian Jiaotong University.

Data availability

Data will be made available on request.

Acknowledgments

We acknowledges the financial support of National Natural Science Foundation of China (12102324 and 11890674), the China Postdoctoral Science Foundation (2021M692573 and 2022T150519) and the Fundamental Research Funds for Central Universities (xzy012022007). The work was carried out at National Supercomputer Center in Tianjin, and the calculations were performed on TianHe-1(A).

Appendix A. Supplementary data

Supplementary material related to this article can be found online at https://doi.org/10.1016/j.eml.2022.101921. It includes information of all stable MXene, the thickness, bond energy, bond length, bond stiffness, strength, the E^{2D} of H-phase and T-phase, the bond strength calculated from COHP, the modification of bond length, correlation plot, the contribution of each term in the formula obtained by SISSO and so on.

References

[1] X. Li, Z. Huang, C.E. Shuck, G. Liang, Y. Gogotsi, C. Zhi, Mxene chemistry, electrochemistry and energy storage applications, Nat. Rev. Chem. (2022) 1–16.
[2] B. Anasori, M.R. Lukatskaya, Y. Gogotsi, 2D metal carbides and nitrides (MXenes) for energy storage, Nat. Rev. Mater. 2 (2) (2017) 1.
[3] M. Naguib, M. Kurtoglu, V. Presser, J. Lu, J. Niu, M. Heon, L. Hultman, Y. Gogotsi, M.W. Barsoum, Two-dimensional nanocrystals produced by exfoliation of Ti_3AlC_2, Adv. Mater. 23 (37) (2011) 4248.
[4] M.R. Lukatskaya, O. Mashtalir, C.E. Ren, Y. Dall'Agnese, P. Rozier, P.L. Taberna, M. Naguib, P. Simon, M.W. Barsoum, Y. Gogotsi, Cation intercalation and high volumetric capacitance of two-dimensional titanium carbide, Science 341 (6153) (2013) 1502.
[5] Y. Teng, P. Liu, L. Fu, X.-Y. Kong, L. Jiang, L. Wen, Bioinspired nervous signal transmission system based on two-dimensional laminar nanofluidics: From electronics to ionics, Proc. Natl. Acad. Sci. USA 117 (29) (2020) 16743.
[6] A. Lipatov, A. Goad, M.J. Loes, N.S. Vorobeva, J. Abourahma, Y. Gogotsi, A. Sinitskii, High electrical conductivity and breakdown current density of individual monolayer $Ti_3C_2T_x$ MXene flakes, Matter 4 (4) (2021) 1413.
[7] J. Lao, K. Zhou, S. Pan, J. Luo, J. Gao, A. Dong, L. Jiang, Spontaneous and selective potassium transport through suspended tailor-cut $Ti_3C_2T_x$ MXene film, ACS Nano 16 (6) (2022) 9142–9149.
[8] M. Naguib, M.W. Barsoum, Y. Gogotsi, Ten years of progress in the synthesis and development of MXenes, Adv. Mater. 33 (39) (2021) 2103393.
[9] A.S. Zeraati, S.A. Mirkhani, P. Sun, M. Naguib, P.V. Braun, U. Sundararaj, Improved synthesis of $Ti_3C_2T_x$ MXenes resulting in exceptional electrical conductivity, high synthesis yield, and enhanced capacitance, Nanoscale 13 (6) (2021) 3572.
[10] S. Wan, X. Li, Y. Chen, N. Liu, Y. Du, S. Dou, L. Jiang, Q. Cheng, High-strength scalable MXene films through bridging-induced densification, Science 374 (6563) (2021) 96.
[11] S. Wan, X. Li, Y. Wang, Y. Chen, X. Xie, R. Yang, A.P. Tomsia, L. Jiang, Q. Cheng, Strong sequentially bridged MXene sheets, Proc. Natl. Acad. Sci. USA 117 (44) (2020) 27154.
[12] H. Ding, Z. Zhen, H. Imtiaz, W. Guo, H. Zhu, B. Liu, Why are most 2D lattices hexagonal? The stability of 2D lattices predicted by a simple mechanics model, Extreme Mech. Lett. 32 (2019) 100507.
[13] Z. Liu, B. Wang, Prediction on the theoretical strength of diamond, *c*-BN, Cu, and CeO_2, AIP Adv. 11 (9) (2021) 095111.
[14] B.C. Wyatt, A. Rosenkranz, B. Anasori, 2D MXenes: Tunable mechanical and tribological properties, Adv. Mater. 33 (17) (2021) 2007973.
[15] Y. Ibrahim, A. Mohamed, A.M. Abdelgawad, K. Eid, A.M. Abdullah, A. Elzatahry, The recent advances in the mechanical properties of self-standing two-dimensional MXene-based nanostructures: Deep insights into the supercapacitor, Nanomaterials 10 (10) (2020) 1916.
[16] A. Lipatov, H. Lu, M. Alhabeb, B. Anasori, A. Gruverman, Y. Gogotsi, A. Sinitskii, Elastic properties of 2D $Ti_3C_2T_x$ MXene monolayers and bilayers, Sci. Adv. 4 (6) (2018) eaat0491.
[17] A. Lipatov, M. Alhabeb, H. Lu, S. Zhao, M.J. Loes, N.S. Vorobeva, Y. Dall'Agnese, Y. Gao, A. Gruverman, Y. Gogotsi, et al., Electrical and elastic properties of individual single-layer $Nb_4C_3T_x$ MXene flakes, Adv. Electron. Mater. 6 (4) (2020) 1901382.
[18] Z. Fu, Q. Zhang, D. Legut, C. Si, T.C. Germann, T. Lookman, S. Du, J.S. Francisco, R. Zhang, Stabilization and strengthening effects of functional groups in two-dimensional titanium carbide, Phys. Rev. B 94 (10) (2016) 104103.
[19] P. Chakraborty, T. Das, D. Nafday, L. Boeri, T. Saha-Dasgupta, Manipulating the mechanical properties of Ti_2C MXene: Effect of substitutional doping, Phys. Rev. B 95 (18) (2017) 184106.
[20] Z. Guo, J. Zhou, C. Si, Z. Sun, Flexible two-dimensional $Ti_{n+1}C_n$ ($n = 1, 2$ and 3) and their functionalized mxenes predicted by density functional theories, Phys. Chem. Chem. Phys. 17 (23) (2015) 15348.
[21] Q. Shao, R. Li, Z. Yue, Y. Wang, E. Gao, Data-driven discovery and understanding of ultrahigh-modulus crystals, Chem. Mater. 33 (4) (2021) 1276.
[22] N. Ran, B. Sun, W. Qiu, E. Song, T. Chen, J. Liu, Identifying metallic transition-metal dichalcogenides for hydrogen evolution through multi-level high-throughput calculations and machine learning, J. Phys. Chem. Lett. 12 (8) (2021) 2102.
[23] E. Gao, R. Li, S. Fang, Q. Shao, R.H. Baughman, Bounds on the in-plane Poisson's ratios and the in-plane linear and area compressibilities for sheet crystals, J. Mech. Phys. Solids 152 (2021) 104409.
[24] C. Qian, K. Zhou, Y. Xiong, X. Chen, Z. Li, High-throughput discovery and investigation of auxetic two-dimensional crystals, Chem. Mater. 34 (10) (2022) 4344.
[25] S. Haastrup, M. Strange, M. Pandey, T. Deilmann, P.S. Schmidt, N.F. Hinsche, M.N. Gjerding, D. Torelli, P.M. Larsen, A.C. Riis-Jensen, et al., The computational 2D materials database: High-throughput modeling and discovery of atomically thin crystals, 2D Mater. 5 (4) (2018) 042002.
[26] J. Zhou, L. Shen, M.D. Costa, K.A. Persson, S.P. Ong, P. Huck, Y. Lu, X. Ma, Y. Chen, H. Tang, et al., 2DMatPedia, an open computational database of two-dimensional materials from top-down and bottom-up approaches, Sci. Data 6 (1) (2019) 1.
[27] K. Choudhary, K.F. Garrity, A.C. Reid, B. DeCost, A.J. Biacchi, A.R.H. Walker, Z. Trautt, J. Hattrick-Simpers, A.G. Kusne, A. Centrone, et al., The joint automated repository for various integrated simulations (JARVIS) for data-driven materials design, Npj Comput. Mater. 6 (1) (2020) 1.
[28] F. Mouhat, F.X. Coudert, Necessary and sufficient elastic stability conditions in various crystal systems, Phys. Rev. B 90 (22) (2014) 224104.
[29] A.C. Rajan, A. Mishra, S. Satsangi, R. Vaish, H. Mizuseki, K.-R. Lee, A.K. Singh, Machine-learning-assisted accurate band gap predictions of functionalized MXene, Chem. Mater. 30 (12) (2018) 4031.
[30] S.K. Nemani, B. Zhang, B.C. Wyatt, Z.D. Hood, S. Manna, R. Khaledialidusti, W. Hong, M.G. Sternberg, S. Sankaranarayanan, B. Anasori, High-entropy 2D carbide MXenes: $TiVNbMoC_3$ and $TiVCrMoC_3$, ACS Nano 15 (8) (2021) 12815.
[31] Z. Du, C. Wu, Y. Chen, Z. Cao, R. Hu, Y. Zhang, J. Gu, Y. Cui, H. Chen, Y. Shi, et al., High-entropy atomic layers of transition-metal carbides (MXenes), Adv. Mater. 33 (39) (2021) 2101473.
[32] R. Li, Q. Shao, E. Gao, Z. Liu, Elastic anisotropy measure for two-dimensional crystals, Extreme Mech. Lett. 34 (2020) 100615.
[33] T. Hu, J. Yang, W. Li, X. Wang, C.M. Li, Quantifying the rigidity of 2D carbides (MXenes), Phys. Chem. Chem. Phys. 22 (4) (2020) 2115.
[34] S. Zeng, G. Li, Y. Zhao, R. Wang, J. Ni, Machine learning–aided design of materials with target elastic properties, J. Phys. Chem. C 123 (8) (2019) 5042.
[35] C. Toher, C. Oses, J.J. Plata, D. Hicks, F. Rose, O. Levy, M. de Jong, M. Asta, M. Fornari, M.B. Nardelli, et al., Combining the AFLOW GIBBS and elastic libraries to efficiently and robustly screen thermomechanical properties of solids, Phys. Rev. Mater. 1 (1) (2017) 015401.
[36] Y.-R. Luo, Comprehensive Handbook of Chemical Bond Energies, CRC Press, 2007.
[37] R. Dronskowski, P.E. Bloechl, Crystal orbital Hamilton populations (COHP): Energy-resolved visualization of chemical bonding in solids based on density-functional calculations, J. Phys. Chem. 97 (33) (1993) 8617.
[38] G. Henkelman, A. Arnaldsson, H. Jónsson, A fast and robust algorithm for Bader decomposition of charge density, Comput. Mater. Sci. 36 (3) (2006) 354.
[39] R. Ouyang, S. Curtarolo, E. Ahmetcik, M. Scheffler, L.M. Ghiringhelli, SISSO: A compressed-sensing method for identifying the best low-dimensional descriptor in an immensity of offered candidates, Phys. Rev. Mater. 2 (8) (2018) 083802.
[40] E. Gao, X. Yuan, S.O. Nielsen, R.H. Baughman, Exploring the bounds on the Young's modulus and gravimetric Young's modulus, Phys. Rev. A 18 (1) (2022) 014044.
[41] J. Frenkel, Zur theorie der elastizitätsgrenze und der festigkeit kristallinischer körper, Z. FÜR Phys. 37 (7) (1926) 572.
[42] A.A. Griffith, VI. The phenomena of rupture and flow in solids, Philos. Trans. R. Soc. London, Ser. A 221 (582–593) (1921) 163.
[43] D. Roundy, C. Krenn, M.L. Cohen, J. Morris Jr., Ideal shear strengths of fcc aluminum and copper, Phys. Rev. Lett. 82 (13) (1999) 2713.

[44] H. Wang, Z. Yao, L. Acauan, J. Kong, B.L. Wardle, Toward MXene interconnects, Matter 4 (5) (2021) 1447.
[45] H. Huang, X. Chu, Y. Xie, B. Zhang, Z. Wang, Z. Duan, N. Chen, Z. Xu, H. Zhang, W. Yang, $Ti_3C_2T_x$ MXene-based micro-supercapacitors with ultrahigh volumetric energy density for all-in-one si-electronics, ACS Nano 16 (3) (2022) 3776.
[46] X.-H. Zha, Q. Huang, J. He, H. He, J. Zhai, J.S. Francisco, S. Du, The thermal and electrical properties of the promising semiconductor MXene Hf_2CO_2, Sci. Rep. 6 (1) (2016) 1.
[47] H. Li, S. Chen, D.W. Boukhvalov, Z. Yu, M.G. Humphrey, Z. Huang, C. Zhang, Switching the nonlinear optical absorption of titanium carbide MXene by modulation of the surface terminations, ACS Nano 16 (1) (2022) 394–404.
[48] X. Liu, M.S. Choi, E. Hwang, W.J. Yoo, J. Sun, Fermi level pinning dependent 2D semiconductor devices: Challenges and prospects, Adv. Mater. (2021) 2108425.
[49] C. Liu, H. Chen, S. Wang, Q. Liu, Y.-G. Jiang, D.W. Zhang, M. Liu, P. Zhou, Two-dimensional materials for next-generation computing technologies, Nat. Nanotechnol. 15 (7) (2020) 545.
[50] M. Maździarz, Comment on 'the computational 2D materials database: High-throughput modeling and discovery of atomically thin crystals', 2D Mater. 6 (4) (2019) 048001.
[51] G. Kresse, J. Furthmüller, Efficient iterative schemes for ab initio total-energy calculations using a plane-wave basis set, Phys. Rev. B 54 (16) (1996) 11169.
[52] G. Kresse, J. Furthmüller, Efficiency of ab-initio total energy calculations for metals and semiconductors using a plane-wave basis set, Comput. Mater. Sci. 6 (1) (1996) 15.
[53] P.E. Blöchl, Projector augmented-wave method, Phys. Rev. B 50 (24) (1994) 17953.
[54] J.P. Perdew, K. Burke, M. Ernzerhof, Generalized gradient approximation made simple, Phys. Rev. Lett. 77 (18) (1996) 3865.
[55] V. Wang, N. Xu, J.C. Liu, G. Tang, W.T. Geng, VASPKIT: A user-friendly interface facilitating high-throughput computing and analysis using VASP code, Comput. Phys. Comm. 267 (2021) 108033.
[56] R. Nelson, C. Ertural, J. George, V.L. Deringer, G. Hautier, R. Dronskowski, LOBSTER: Local orbital projections, atomic charges, and chemical-bonding analysis from projector-augmented-wave-based density-functional theory, J. Comput. Chem. 41 (21) (2020) 1931.
[57] C. Chen, X. Ji, K. Xu, B. Zhang, L. Miao, J. Jiang, Prediction of T- and H-phase two-dimensional transition-metal carbides/nitrides and their semiconducting–metallic phase transition, ChemPhysChem 18 (14) (2017) 1897.